Materials Research Letters

ISSN: (Print) 2166-3831 (Online) Journal homepage: http://www.tandfonline.com/loi/tmrl20

Low temperature structural stability of $Fe_{90}Sc_{10}$ nanoglasses

Chaomin Wang, Tao Feng, Di Wang, Xiaoke Mu, Mohammad Ghafari, Ralf Witte, Aaron Kobler, Christian Kübel, Yulia Ivanisenko, Herbert Gleiter & Horst Hahn

To cite this article: Chaomin Wang, Tao Feng, Di Wang, Xiaoke Mu, Mohammad Ghafari, Ralf Witte, Aaron Kobler, Christian Kübel, Yulia Ivanisenko, Herbert Gleiter & Horst Hahn (2018) Low temperature structural stability of $Fe_{90}Sc_{10}$ nanoglasses, Materials Research Letters, 6:3, 178-183, DOI: 10.1080/21663831.2018.1430622

To link to this article: https://doi.org/10.1080/21663831.2018.1430622

MATER. RES. LETT., 2018
VOL. 6, NO. 3, 178–183
https://doi.org/10.1080/21663831.2018.1430622

MATERIALS RESEARCH LETTERS
Taylor & Francis
Taylor & Francis Group

ORIGINAL REPORTS

Low temperature structural stability of $Fe_{90}Sc_{10}$ nanoglasses

Chaomin Wang[a,b], Tao Feng[c], Di Wang[a,d], Xiaoke Mu[a,e], Mohammad Ghafari[c], Ralf Witte[a,b], Aaron Kobler[a,b], Christian Kübel[a,d,e], Yulia Ivanisenko[a], Herbert Gleiter[a,c] and Horst Hahn[a,b,c]

[a]Institute of Nanotechnology, Karlsruhe Institute of Technology, Eggenstein-Leopoldshafen, Germany; [b]KIT-TUD Joint Research Laboratory Nanomaterials, Technische Universität Darmstadt, Darmstadt, Germany; [c]Herbert Gleiter Institute of Nanoscience, Nanjing University of Science and Technology, Nanjing, People's Republic of China; [d]Karlsruhe Nano Micro Facility, Karlsruhe Institute of Technology, Eggenstein-Leopoldshafen, Germany; [e]Helmholtz Institute Ulm, Karlsruhe Institute of Technology, Eggenstein-Leopoldshafen, Germany

ABSTRACT

The structural stability of $Fe_{90}Sc_{10}$ nanoglasses has been studied by means of low temperature crystallization. Specimens were annealed *in situ* in a transmission electron microscope, and *ex situ* in an ultra-high vacuum tube-furnace. Both studies led to similar results. The structure of the $Fe_{90}Sc_{10}$ nanoglasses was stable for up to 2 h when annealed at 150°C. Annealing the $Fe_{90}Sc_{10}$ nanoglasses at higher temperature resulted in the formation of the nanocrystalline bcc-Fe(Sc).

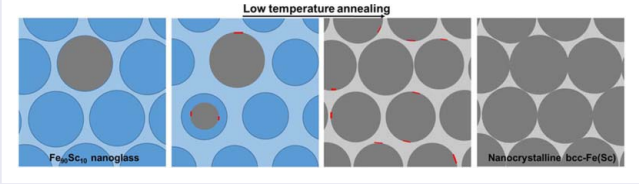

IMPACT STATEMENT

The structural evolution of $Fe_{90}Sc_{10}$ nanoglasses has been studied in detail during low temperature annealing. Our results indicate that the nanostructure of $Fe_{90}Sc_{10}$ nanoglasses is quite stable at low temperature.

ARTICLE HISTORY
Received 7 August 2017

KEYWORDS
Nanoglasses; structural stability; interfaces; low temperature annealing

Nanoglasses (NGs) [1,2] are nanostructured non-crystalline materials, which are most frequently prepared by consolidation of glassy nanoparticles. The atomic structure of NGs was proposed to consist of nanometer-sized glassy regions (glassy cores) with interfacial regions (interfaces) between them. The interfaces within NGs are expected to consist of lower atomic packing density areas with larger inter-atomic distances compared to the corresponding melt-quenched glasses with the identical chemical compositions. Recent studies also indicate that the chemical composition and the short-range order (SRO) of the interfaces differ from the composition and SRO of the cores [3–9]. Due to the presence of these interfaces, NGs exhibit properties, which differ from the corresponding melt-quenched metallic glasses (MQMG) with comparable chemical compositions [4,10,11]. For instance, at room temperature, $Fe_{90}Sc_{10}$ NGs are ferromagnetic while $Fe_{90}Sc_{10}$ melt-spun ribbons are paramagnetic. The room-temperature ferromagnetism of the $Fe_{90}Sc_{10}$ NGs was attributed to the interfaces with different electronic structure [10,12].

Since the properties of materials are determined by their atomic structures and their microstructures, it is important to study the structural stability. For NGs, several computer simulations have been performed to investigate the structural stability. For example, Albe et al. [3,5] simulated the structural evolution of NG during annealing, and found that the free volume within the interfaces of the as-prepared NG can delocalize, so that the volume fraction of the interfaces increases. Due to this delocalization process, the free volume localized initially in the NG interfaces spreads out over the entire sample, resulting in a structure of nearly homogeneous density distribution. In these computations, the inter-atomic interaction

CONTACT Chaomin Wang chaomin.wang@partner.kit.edu; Herbert Gleiter herbert.gleiter@kit.edu; Horst Hahn horst.hahn@kit.edu
Institute of Nanotechnology, Karlsruhe Institute of Technology, 76344 Eggenstein-Leopoldshafen, Germany

Supplemental data for this article can be accessed here. https://doi.org/10.1080/21663831.2018.1430622

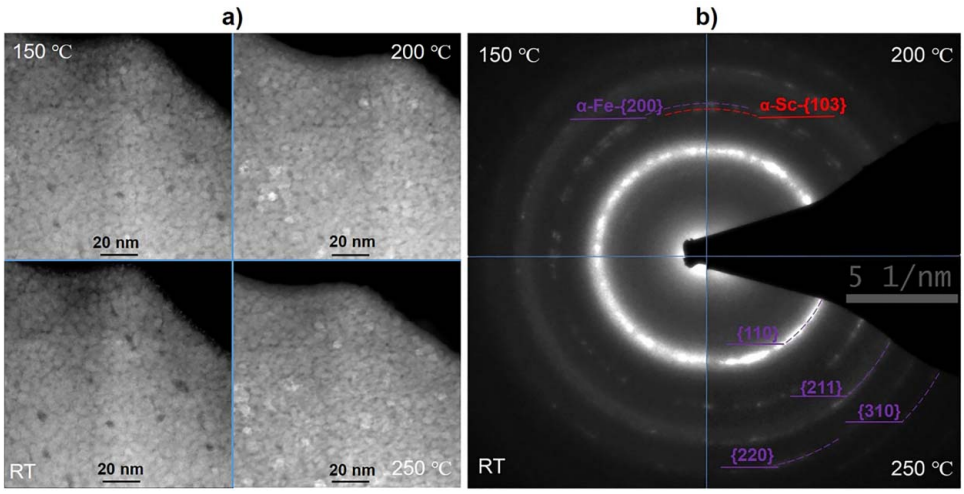

Figure 1. STEM images and ED patterns of an $Fe_{90}Sc_{10}$ NG lamella annealed *in situ*. (a) STEM images, (b) ED patterns corresponding to the STEM images.

was assumed to be the same in the interfaces and in the cores. However, the structural evolution of NGs is difficult to be characterized experimentally, since the atomic structure of the interfaces is disordered and the thickness of the interfaces is in the nanometer range. Accordingly, the experimental results of the structural stability of NGs were rare.

In the present work, using Mössbauer spectroscopy (MS), scanning transmission electron microscopy (STEM) and electron diffraction (ED), the local information of the structural evolution of $Fe_{90}Sc_{10}$ NGs could be recorded during low temperature annealing. The experimental results obtained seem to provide an improved understanding of the structural stability of NGs.

$Fe_{90}Sc_{10}$ glassy nanoparticles were prepared by inert gas condensation [4,13] and were consolidated in the inert gas condensation device into disc-shaped NG pellets at two GPa. This preparation step was followed by a second consolidation step at six GPa using a high-pressure torsion device.

Annealing of the NG pellet was performed in an ultra-high vacuum (UHV) tube-furnace at a pressure of 1×10^{-8} mbar. During one annealing experiment, the same pellet was heated from room temperature to the desired temperatures (150°C, 200°C and 250°C) and annealed for 2 h at each temperature. In between, X-ray diffraction (XRD) patterns were recorded at room temperature using a Philips X'Pert Panalytical diffractometer using Mo-Kα radiation (step size = 0.02°, the integration time was 15 s/step.). Prior to the start of the X-ray scan, the height of the sample substrate was carefully calibrated to determine the exact position and intensity of the diffraction peaks. MS was performed using a standard transmission setup with a ^{57}Co Rh source and linear acceleration mode at 20 K.

Thin $Fe_{90}Sc_{10}$ NG lamellas required for STEM and ED analysis were prepared by focused ion beam (FIB, FEI Strata 400 S) cutting from the NG pellets and finally thinned using a Fischione NanoMill 1040 which was equipped with Liquid nitrogen-cooled specimen stage. To avoid sample heating, NanoMill was used with Ar^+ ions at low voltage of 600 V. The Ga^+ ions implanted surface layer of the primary FIB samples could be removed by the Ar^+ ions. The *in situ* annealing experiments were performed using an aberration (image) corrected FEI Titan 80–300 electron microscope (FEI Co., Hillsboro, OR, USA), which was operated at an accelerating voltage of 300 kV in nanoprobe mode for STEM imaging and in TEM mode for ED acquisition. The lamellas were heated up to the desired temperatures with a constant heating rate of 5°C/s. After annealing them at 150°C, 200°C and 250°C for half an hour at each temperature, the STEM and ED patterns of these $Fe_{90}Sc_{10}$ lamellas were recorded.

The STEM images and ED patterns of the $Fe_{90}Sc_{10}$ NG specimens that were annealed in the transmission electron microscopy are displayed in Figure 1. The STEM images (Figure 1(a)) reveal that the specimens keep their granular appearance. In fact, no change in the size of the 'nanograins' was noted during annealing indicating the stability of the nanostructure of $Fe_{90}Sc_{10}$ samples [8,10].

The ED patterns (Figure 1(b)) corresponding to the STEM images show the structural evolution of the $Fe_{90}Sc_{10}$ NG samples. Briefly, the $Fe_{90}Sc_{10}$ NG lamella crystallize into a metastable nanocrystalline bcc-Fe (Sc) when it was heated from room temperature to 250°C. During this process, some α-Sc nanocrystallites were semi-coherently precipitated from the bcc-Fe(Sc)

nanocrystallites [14], which were identified by the extra diffraction rings near the {200} diffraction rings of the bcc-Fe(Sc) nanocrystallites (see '150°C' and '200°C' ED patterns). The phase attribution of the extra diffraction rings is given in the supplemental material-1 (SM-1).

The Mössbauer spectra of the $Fe_{90}Sc_{10}$ NG pellet, which was annealed in an UHV tube-furnace are shown in Figure 2(a). The spectrum of the as-prepared $Fe_{90}Sc_{10}$ NG pellet (Figure 2(a-RT)) could be fitted with three components [10,12], corresponding to the glassy cores with the similar structure as the corresponding melt-spun ribbons (green sub-spectrum), interfaces with enhanced free volume (blue sub-spectrum) and a small amount of bcc-Fe nanocrystallites (red sub-spectrum). The area fraction of the sub-spectrum is proportional to the relative amount (percentage) of the Fe atoms.

After annealing at 150°C for 2 h, it was found that the relative amount of the Fe atoms of the cores decreased and simultaneously the content of the bcc-Fe nanocrystallites increased (Figure 2(a-150°C)). The XRD analysis (Figure 2(b-150°C)) confirms the increased content of bcc-Fe nanocrystallites. No α-Sc nanocrystallites were detected by XRD, which may be due to their small size and their small volume fraction. During annealing, the relative amount of the Fe atoms of the interfaces was noted to increase, which is indicated by the increased area fraction of the blue sub-spectrum.

The glassy cores were completely crystallized after annealing at 200°C for 2 h, as shown in Figure 2(a-200°C). This crystallization is indicated by the disappearance of the green sub-spectrum. Although trace of the blue sub-spectrum originating from the interfaces still exists at 200°C. However, compared to 150°C, the isomer shift is smaller. The decline of the isomer shift indicates an enhanced electronic density of interfaces. Also considering the STEM image (Figure 1(a-200°C)) and the XRD pattern (Figure 2(b-200°C)), we are led to conclude that the blue sub-spectrum in Figure 2(b-200°C) characterizes the interfaces within the nanocrystalline bcc-Fe(Sc) [15]. Compared with the interfaces within the $Fe_{90}Sc_{10}$ nanoglasses, the interfaces within the nanocrystalline bcc-Fe(Sc) are thinner and have more ordered structure with less free volume.

During further annealing of the specimen, the area fraction of the blue sub-spectrum decreased (Figure 2(a-250°C)) which indicates that the relative amount of the Fe atoms of the interfaces decreases. This might due to the decrease of the volume fraction of the interfaces and the enrichment of the Sc atoms of the interfaces. In fact, the first peak of the XRD pattern shifts towards higher angle (see the insert in Figure 2(b)), which suggests that some Sc atoms diffuse out of the lattices of

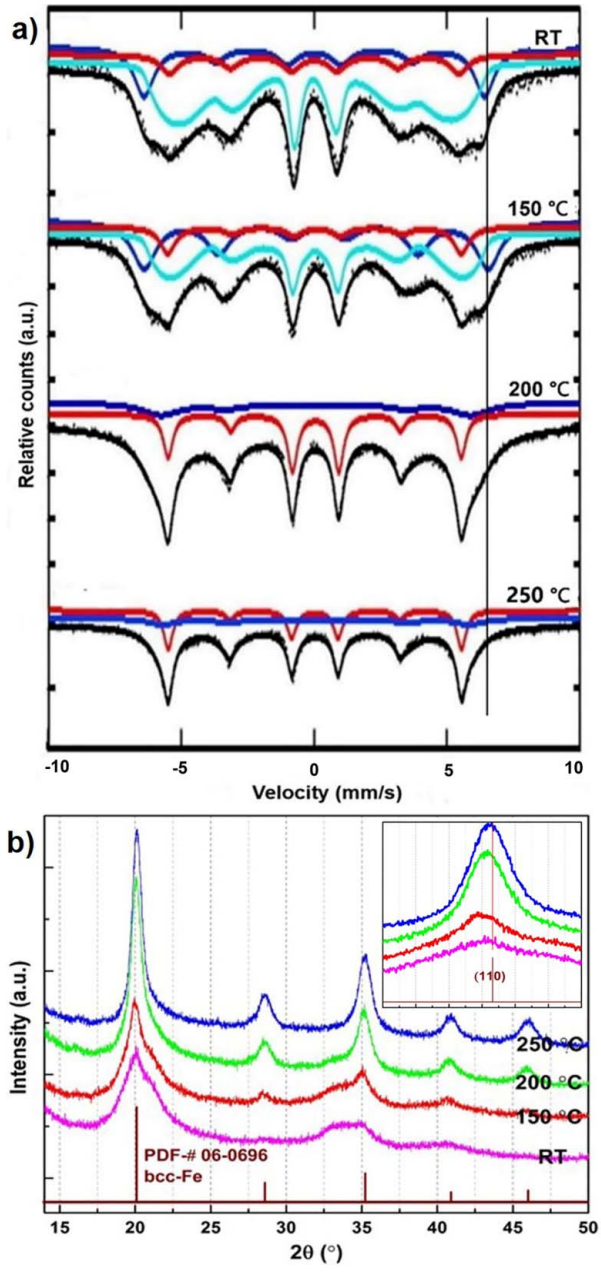

Figure 2. Mössbauer spectra and XRD patterns of $Fe_{90}Sc_{10}$ NG during annealing in UHV tube-furnace. (a) Low temperature Mössbauer spectra which were recorded at 20 K. (b) XRD patterns corresponding to the Mössbauer spectra. The original Mössbauer spectra were fitted with different sub-spectrums [10,12]. The red sub-spectrum represent the bcc-Fe nanocrystallites, the blue sub-spectrum represent interfacial regions (interfaces), while the green sub-spectrum represent the glassy cores.

bcc-Fe(Sc) nanocrystallites (crystalline cores) and segregate to the interfaces. Additional information about the α-Sc nanocrystallites and the nanocrystalline bcc-Fe(Sc) is given in SM-2.

By combining the results reported so far, the structural model shown in Figure 3 for the crystallization process of $Fe_{90}Sc_{10}$ NGs was obtained. Specifically, Figure 3(a)

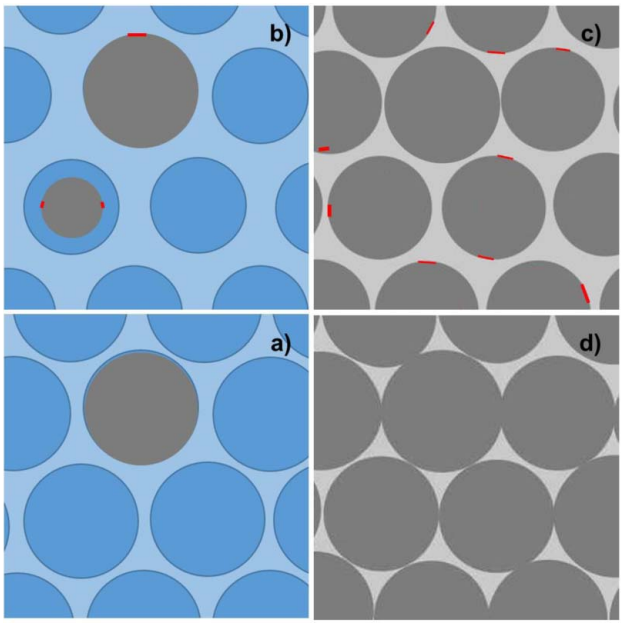

Figure 3. Schematic drawing of the structural evolution of $Fe_{90}Sc_{10}$ NGs during low temperature annealing. (a) As-prepared $Fe_{90}Sc_{10}$ NG, (b) after annealing at 150°C for some time, (c) after annealing at 200°C for some time, (d) after annealing at 250°C for some time. Dark-blue spheres represent the glassy cores within the $Fe_{90}Sc_{10}$ NG, light-blue background represents the interfaces within the $Fe_{90}Sc_{10}$ NG. Dark-gray spheres represent the bcc-Fe(Sc) nanocrystallites (crystalline cores), light-gray background represents the interfaces within the nanocrystalline bcc-Fe(Sc). The red slices at boundaries of dark-gray spheres represent the metastable α-Sc nanocrystallites.

represents the as-prepared $Fe_{90}Sc_{10}$ NG which consists of cores (dark-blue spheres), interfaces (light-blue background) and some primary bcc-Fe(Sc) nanocrystallites (gray sphere). The Sc concentration of the interfaces is lower than within the cores [8]. After annealing at 150°C (Figure 3(b)), the relative amount of the Fe atoms of the interfaces increases, which also means that the free volume within the interfaces delocalize to the glassy cores [4]. Some small metastable α-Sc nanocrystallites (red slices at the boundaries of gray spheres) are precipitated from the bcc-Fe(Sc) nanocrystallites [14]. Annealing at 200°C (Figure 3(c)) causes all the glassy cores within the $Fe_{90}Sc_{10}$ NG to crystallize into crystalline cores (bcc-Fe(Sc) nanocrystallites). The light-gray background represents the interfaces with enhanced atomic density. Increasing the annealing temperature to 250°C (Figure 3(d)), causes the metastable α-Sc nanocrystallites to segregate to the interfaces and the volume fraction of the interfaces is reduced.

Figure 4(a) shows the radial distribution functions (RDFs) of the $Fe_{90}Sc_{10}$ samples calculated from the ED patterns using the method described in ref. [16]. Figure 4(b) displays the computer simulated RDFs of liquid Fe during cooling [17]. The similarity of both curves suggests that the structure of the as-prepared $Fe_{90}Sc_{10}$ NG resembles the structure of liquid Fe at 1250 K (see the higher resolution curves in SM-3). This result agrees with the observations of Ghafari et al. [18]. They concluded that $Fe_{90}Sc_{10}$ melt-spun ribbons contain a high density of distorted bcc-Fe (bcc-Fe like) clusters on the basis of the similarity of RDFs of the $Fe_{90}Sc_{10}$ melt-spun ribbons and bcc-Fe crystals. Hirata et al. [19] deduced plausible structure models for Fe-based MQMG using ED intensity analysis with the help of reverse Monte Carlo simulation. In fact, they also proposed that bcc-Fe like clusters are the dominant feature of the SRO of Fe-based MQMG, and the ratio of bcc-Fe like clusters increases with increasing the Fe concentration.

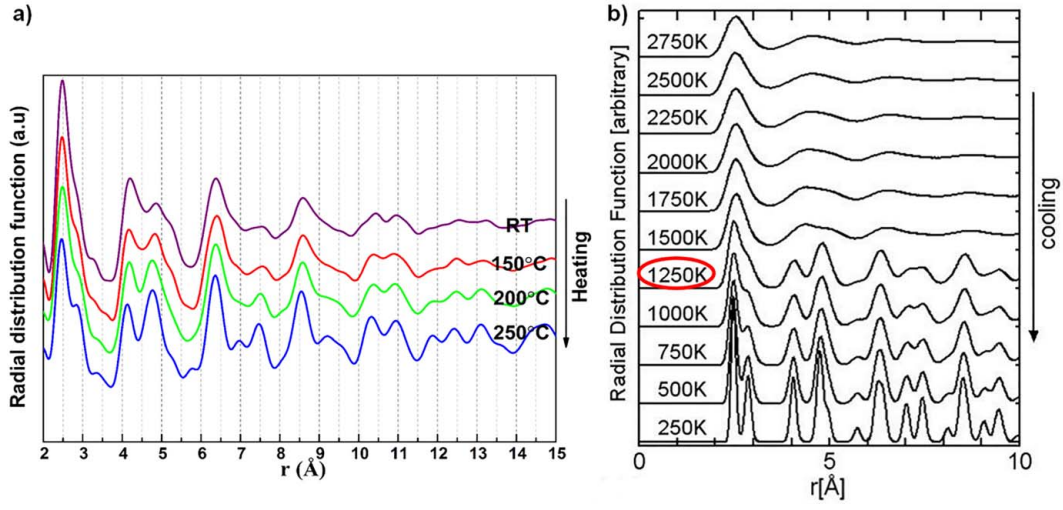

Figure 4. RDFs revealing the structural evolution of $Fe_{90}Sc_{10}$ NG during *in situ* annealing (a), and computer simulated RDFs for the structural evolution of liquid Fe during cooling (b) [17].

The similarity between the RDFs of NG during the heating process and RDFs of liquid Fe during the cooling process is also suggested by the following observation. As shown in Figure 4(b), with decreasing temperature, the shoulder of the first peak of the RDF at 1250 K gradually separates into two individual peaks. The newly formed peak corresponds to the second coordination sphere of the ordered bcc-Fe structure. In other words, the separation of the shoulder indicates an increasingly defined structure of bcc-Fe like clusters ultimately corresponding to the structure of an ordered bcc-Fe crystal. According to Pan [20] and Shibuta [17], the enlargement of the coordination number, which is indicated as the separation of the shoulders, is a typical and necessary route from bcc-Fe like clusters to long-range ordered bcc-Fe crystal. For the $Fe_{90}Sc_{10}$ NG, the separation of the shoulder can also be observed. However, the shoulder does not separate fully, which may be due to a superposition of distances corresponding to Fe-Fe and Fe-Sc pairs [21].

It has been reported that low temperature crystallization of Fe-based MQMG is a polymorphous crystallization process by growing of clusters with critical size [22–25]. These ordered clusters are formed during the quenching process and can serve as pre-existing nuclei that grow into nanocrystallites by rearranging the atoms in short-range [26,27]. Thus, the structure of these nanocrystallites are close to the structure of the ordered clusters. For example, after annealing at low temperature for a long time, $Fe_{80}P_{13}C_7$ and $Fe_{78}Si_{10}B_{12}$ MQMG can also be crystallized into the nanocrystalline bcc-Fe [22].

In summary, all of these results seem to suggest that the $Fe_{90}Sc_{10}$ NG mainly consists of bcc-Fe like clusters [28], and the low temperature crystallization processes of the $Fe_{90}Sc_{10}$ NG is initiated by rearranging the atoms of the bcc-Fe like clusters to form nanocrystalline bcc-Fe (Sc).

Acknowledgement

Wang CM gratefully acknowledges the support of the China Scholarship Council (CSC).

Disclosure statement

No potential conflict of interest was reported by the authors.

Funding

This work was supported by the Deutsche Forschungsgemeinschaft [grant number HA1344/30-1]; National Natural Science Foundation of China [grant number 51571119, 51520105001].

References

[1] Gleiter H. Our thoughts are ours, their ends none of our own: are there ways to synthesize materials beyond the limitations of today? Acta Mater. 2008;56:5875–5893.
[2] Gleiter H, Schimmel T, Hahn H. Nanostructured solids – from nano-glasses to quantum transistors. Nano Today. 2014;9:17–68.
[3] Ritter Y, Şopu D, Gleiter H, et al. Structure, stability and mechanical properties of internal interfaces in CuZr nanoglasses studied by MD simulations. Acta Mater. 2011;59:6588–6593.
[4] Fang JX, Vainio U, Puff W, et al. Atomic structure and structural stability of $Sc_{75}Fe_{25}$ nanoglasses. Nano Lett. 2012;12:458–463.
[5] Sopu D, Albe K, Ritter Y, et al. From nanoglasses to bulk massive glasses. Appl Phys Lett. 2009;94:191911.
[6] Danilov D, Hahn H, Gleiter H, et al. Mechanisms of nanoglass ultrastability. ACS Nano. 2016;10:3241–3247.
[7] Adjaoud O, Albe K. Interfaces and interphases in nanoglasses: surface segregation effects and their implications on structural properties. Acta Mater. 2016;113:284–292.
[8] Wang CM, Wang D, Mu XK, et al. Surface segregation of primary glassy nanoparticles of $Fe_{90}Sc_{10}$ nanoglass. Mater Lett. 2016;181:248–252.
[9] Wang CM, Guo XA, Ivanisenko Y, et al. Atomic structure of $Fe_{90}Sc_{10}$ glassy nanoparticles and nanoglasses. Scripta Mater. 2017;139:9–12.
[10] Witte R, Feng T, Fang JX, et al. Evidence for enhanced ferromagnetism in an iron-based nanoglass. Appl Phys Lett. 2013;103:073106.
[11] Wang XL, Jiang F, Hahn H, et al. Sample size effects on strength and deformation mechanism of $Sc_{75}Fe_{25}$ nanoglass and metallic glass. Scripta Mater. 2016;116:95–99.
[12] Ghafari M, Hahn H, Gleiter H, et al. Evidence of itinerant magnetism in a metallic nanoglass. Appl Phys Lett. 2012;101:243104.
[13] Feng T, Wang D, Wang CM, et al. Generating metallic amorphous core-shell nanoparticles by a solid-state amorphization process. Part Part Syst Charact. 2016;33:82–88.
[14] Nageswararao M, Herman H, Mcmahon CJ. On the decomposition of supersaturated Fe-Sb, Fe-Sn, and Fe-Sb-Ni solid solutions. Metal Sci. 1976;10:249–252.
[15] Herr U, Jing J, Birringer R, et al. Investigation of nanocrystalline iron materials by Mössbauer spectroscopy. Appl Phys Lett. 1987;50:472–474.
[16] Mu XK, Neelamraju S, Sigle W, et al. Evolution of order in amorphous-to-crystalline phase transformation of MgF_2. J Appl Crystallogr. 2013;46:1105–1116.
[17] Shibuta Y, Suzuki T. A molecular dynamics study of the phase transition in bcc metal nanoparticles. J Chem Phys. 2008;129:144102.
[18] Ghafari M, Gleiter H, Feng T, et al. Are transition metal-rich metallic glasses made up of distorted BCC clusters? J Mater Sci Eng. 2016;5:1000299.
[19] Hirata A, Hirotsu Y. Structure analyses of Fe-based metallic glasses by electron diffraction. Materials. 2010;3:5263–5273.
[20] Pan SP, Feng SD, Qiao JW, et al. Crystallization pathways of liquid-bcc transition for a model iron by fast quenching. Sci Rep. 2015;5:1975.
[21] Ghafari M, Kohara S, Hahn H, et al. Structural investigations of interfaces in $Fe_{90}Sc_{10}$ nanoglasses using

high-energy X-ray diffraction. Appl Phys Lett. 2012;100: 133111.
[22] Masumoto T, Kimura H, Inoue A, et al. Structural stability of amorphous metals. Mater Sci Eng. 1976;23:141–144.
[23] Kulik T, Ferenc J, Matyja H. Low temperature nanocrystallization of iron-based amorphous alloys. Mater Sci Forum. 1997;235-238:421–426.
[24] Waseda Y, Okazaki H, Masumoto T. Current views on the structure and crystallization of metallic glasses. J Mater Sci. 1977;12:1927–1949.
[25] Kulik T. Nanocrystallization of metallic glasses. J Non-Cryst Solids. 2001;287:145–161.
[26] Kelton KF, Greer AL, Herlach DM, et al. The influence of order on the nucleation barrier. MRS Bull. 2004;29:940–944.
[27] Liu XJ, Chen GL, Hou HY, Hui X, Yao KF, Lu ZP, et al. Atomistic mechanism for nanocrystallization of metallic glasses. Acta Mater. 2008;56:2760–2769.
[28] Louzguine-Luzgin DV, Hahn H, Gleiter H, et al. To be published.